The Astrophysical Journal Supplement Series, 239:2 (15pp), 2018 November https://doi.org/10.3847/1538-4365/aae3e9

A Revised Exoplanet Yield from the *Transiting Exoplanet Survey Satellite* (*TESS*)

Thomas Barclay[1,2], Joshua Pepper[3], and Elisa V. Quintana[1]
[1] NASA Goddard Space Flight Center, 8800 Greenbelt Road, Greenbelt, MD 20771, USA
[2] University of Maryland, Baltimore County, 1000 Hilltop Circle, Baltimore, MD 21250, USA
[3] Department of Physics, Lehigh University, 16 Memorial Drive East, Bethlehem, PA 18015, USA
Received 2018 April 14; revised 2018 August 17; accepted 2018 August 27; published 2018 October 25

Abstract

The *Transiting Exoplanet Survey Satellite* (*TESS*) has a goal of detecting small planets orbiting stars bright enough for mass determination via ground-based radial velocity observations. Here, we present estimates of how many exoplanets the *TESS* mission will detect, the physical properties of the detected planets, and the properties of the stars that those planets orbit. This work uses stars drawn from the *TESS* Input Catalog Candidate Target List and revises yields from prior studies that were based on Galactic models. We modeled the *TESS* observing strategy to select approximately 200,000 stars at 2-minute cadence, while the remaining stars are observed at 30-minute cadence in full-frame image data. We placed zero or more planets in orbit around each star, with physical properties following measured exoplanet occurrence rates, and used the *TESS* noise model to predict the derived properties of the detected exoplanets. In the *TESS* 2-minute cadence mode we estimate that *TESS* will find 1250 ± 70 exoplanets (90% confidence), including 250 smaller than 2 $R_\oplus$. Furthermore, we predict that an additional 3100 planets will be found in full-frame image data orbiting bright dwarf stars and more than 10,000 around fainter stars. We predict that *TESS* will find 500 planets orbiting M dwarfs, but the majority of planets will orbit stars larger than the Sun. Our simulated sample of planets contains hundreds of small planets amenable to radial velocity follow-up, potentially more than tripling the number of planets smaller than 4 $R_\oplus$ with mass measurements. This sample of simulated planets is available for use in planning follow-up observations and analyses.

Key words: catalogs – methods: statistical – planetary systems – surveys

Supporting material: machine-readable table

1. Introduction

While we have known that planets orbit stars other than the Sun since the late twentieth century (Campbell et al. 1988; Latham et al. 1989; Wolszczan & Frail 1992; Mayor & Queloz 1995), it is only with the launch of the *Kepler* spacecraft in 2009 (Borucki et al. 2010; Koch et al. 2010) that we have been able to estimate the occurrence rates of terrestrial worlds. While there is not a firm consensus on the details of how common planets are as a function of size and orbital period (Gould et al. 2010; Howard et al. 2010; Catanzarite & Shao 2011; Youdin 2011; Howard et al. 2012; Traub 2012; Bonfils et al. 2013; Fressin et al. 2013; Petigura et al. 2013a, 2013b; Swift et al. 2013; Kane et al. 2014; Foreman-Mackey et al. 2014; Montet et al. 2014; Burke et al. 2015; Clanton & Gaudi 2016; Hsu et al. 2018), it is clear that exoplanets overall are fairly commonplace, particularly orbiting the coolest of stars (Dressing & Charbonneau 2013, 2015; Morton & Swift 2014; Mulders et al. 2015).

Although we have a fairly large sample of planets with orbital periods of less than a few hundred days, there is still a pressing need to detect planets that are readily characterizable. The primary goal of the *Transiting Exoplanet Survey Satellite* (*TESS*), a mission led by the Massachusetts Institute of Technology, is to find small planets that are most amenable for mass measurements through precise radial velocity (RV) observations (Ricker et al. 2015, 2016; Collins et al. 2018). A secondary, although unofficial, mission goal is to find targets that can be characterized through transmission spectroscopy from the *James Webb Space Telescope* (*JWST*) and other future observatories.

TESS launched on 2018 April 18 and resides in an elliptical 13.7-day high-Earth orbit during a 2 yr primary mission. *TESS* has four cameras, each with a 24° × 24° field of view. The cameras are aligned to provide continuous coverage of 96° × 24°, which is maintained for 27.4 days per pointing (known as a sector). The long axis of the observing region is aligned with a fixed ecliptic longitude, with the boresight of the fourth camera centered on the ecliptic pole, as shown in Figure 1. Every two orbits, *TESS* rotates ∼28° about the ecliptic pole. In year 1 of the mission, the spacecraft will survey 13 sectors in the southern ecliptic hemisphere, before spending year 2 in the northern ecliptic hemisphere. About 60% of the sky will be covered by a single sector of *TESS* observations, and a further 15% will be observed over two sectors, located in the overlap areas between two adjacent sectors. Most stars within 12° of the ecliptic poles will be within the *TESS* continuous viewing zone (CVZ) and observable for more than 300 days (this accounts for approximately 1% of the sky per pole). Over the course of the prime mission, *TESS* will observe approximately 85% of the sky.

The *TESS* mission is focused on detecting small transiting planets that orbit bright stars. Although the dwell time over most of the sky is too short to permit the detection of planets in temperate orbits, that goal can be advanced by discovering planets orbiting cooler stars, especially in the *TESS* CVZ around the ecliptic poles.

Two observing modes will be initially implemented: the 96° × 24° full-frame image (FFI) will be recorded every 30 minutes, while approximately 200,000 stars will be

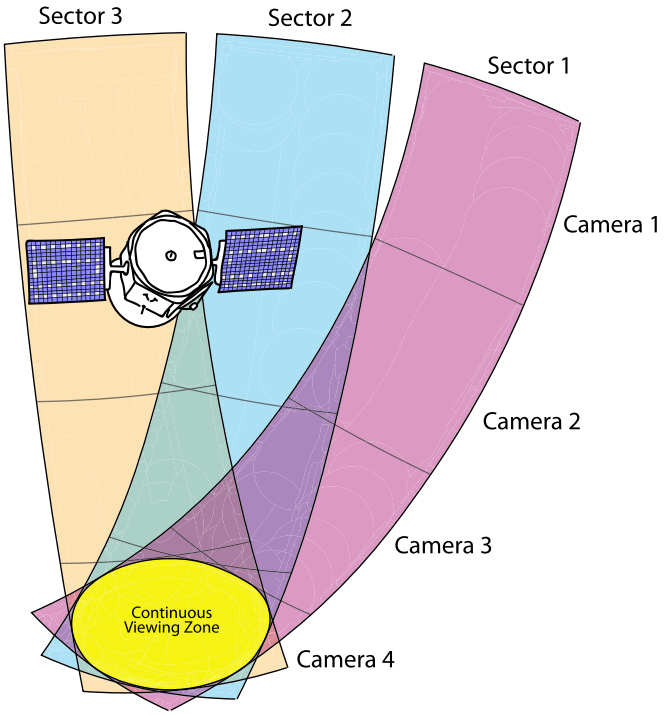

Figure 1. Illustration showing the first three sectors of the *TESS* observing plan.

preselected to have data recorded at 2-minute cadence. In either case, the system is integrating and reading out every 2 s; they differ in the number of co-adds.

It is essential that a *reasonable* prediction for the scientific yield of *TESS* is available because (a) planning follow-up resources requires knowing the properties of the planets we might find (Crouzet et al. 2017; Collins et al. 2018; Kempton et al. 2018; Louie et al. 2018), (b) we can perform trade studies on target prioritization schemes for the 2-minute cadence targets (Bouma et al. 2017; Stassun et al. 2017, J. Pepper et al. 2018, in preparation) and when designing data analysis algorithms (Kipping & Lam 2017; Lund et al. 2017; Vinícius et al. 2017; Oelkers & Stassun 2018), and (c) we can manage the expectations of the scientific community and the public.

A *TESS* yield simulation created by Sullivan et al. (2015) has been the standard used by both the mission team and the community. Since then, two papers have built on the work of Sullivan et al. to refine the total mission yield and explore extended mission scenarios (Bouma et al. 2017) and to improve estimates of the planet yield from M dwarfs (Ballard 2018). However, Sullivan et al. (2015) simulations were based on a simulated stellar population rather than real stars and used an earlier hardware configuration that provided for greater storage and downlink limits than the flight hardware being used. Therefore, now is the time to revise the *TESS* yield estimate using new information. Here, we report on a new estimate of the exoplanet yield using the *TESS* Input Catalog (TIC) Candidate Target List (CTL), the same list that is used by the mission to select stars and perform photometry.

2. Simulating Stars, Planets, and Detections

The process we used to derive a population of planets detectable by *TESS* uses a Monte Carlo method to (1) simulate the population of stars that *TESS* will observe, (2) place planets in orbit around these stars, and (3) predict how many of these planets *TESS* will detect.

2.1. Star Selection

The first step was made relatively straightforward by the availability of the CTL—a prioritized list of target stars that the *TESS* Target Selection Working Group has determined represent the stars most suitable for detection of small planets by *TESS*. The properties of about 500 million stars were assembled in the TIC (Stassun et al. 2017), and the CTL includes several million of those stars that are most suitable for small transit detection. We used CTL version 6.1,[4] which includes 3.8 million stars with properties such as stellar radii, masses, distances, and apparent brightness in various bandpasses. The CTL stars were then ranked using a simple metric based on stellar brightness and radius, along with the degree of blending and flux contamination (especially important given the large *TESS* pixels). The CTL does not include all stars. Save for stars on specially curated target lists (e.g., Muirhead et al. 2018), stars with reduced proper motions (RPMs) that indicate they are red giants (Collier Cameron et al. 2007), stars with a temperature below 5500 K and a *TESS* magnitude fainter than 12, or stars with temperature above 5500 K and a *TESS* magnitude fainter than 13 are excluded from the CTL. Such broad cuts were required in order to assemble a small enough population of stars to practically manage.

We then determined which of these stars are likely to be observed by the mission. We used *tvguide* (Mukai & Barclay 2017) on each star to determine whether and for how long it is observable with *TESS*. We arbitrarily selected a central ecliptic longitude for the first sector of 277°, which equates to an antisolar date of June 28 (the precise timing of the first sector is dependent on commissioning duration). Until we have on-orbit measurements of focal plane geometry, *tvguide* assumes that the cameras are uniform square detectors projected on the sky, placed precisely 24° apart in ecliptic latitude and with identical ecliptic longitude. Gaps between CCDs are assumed to be 0°.25. We ended up with a total of 3.18 million individual stars on silicon.

We also needed to simulate which of these stars are likely to be observed at 2-minute cadence and ensure compliance with the *TESS* mission requirement that states that over the 2 yr mission more than 200,000 total stars should be targeted, and 10,000 stars should be observed for at least 120 days. It is somewhat less trivial than one would initially assume to simulate this requirement because we could not simply select the top 200,000 stars with the highest priority in the CTL because this would place far too many stars in the CVZ than can actually be observed there at 2-minute cadence. To ensure a realistic distribution of targets, we first divided each ecliptic hemisphere into 15 sections: a polar section with everything within 13° of the pole, representing stars that primarily fall into Camera 4; an ecliptic section including everything within 6° of the ecliptic to represent stars that are not observed in the prime mission; and then the remaining area was divided longitudinally into 13 northern and 13 southern adjacent sections, representing stars observable with Cameras 1–3 in Sectors 1–26. This yielded a total of 28 sections of the sky with observable stars.

[4] The TIC and CTL are available from the MAST archive at http://archive.stsci.edu/tess/.

A star that fell in a camera overlap region is observed in multiple sectors but only represented one unique target. We found that we could make a reasonable approximation to satisfy the requirements of 200,000 unique targets if in each polar section we selected the 6000 stars in that region with the highest priority in the CTL, and then for each longitudinal section (representing the footprint of Cameras 1–3 in each sector) we selected the 8,200 highest-priority stars in each of the regions. After removing stars that fall into CCD and camera gaps, this yielded 214,000 unique stars. We assumed that any star in an overlap region is observed in every possible sector. Figure 2 shows the breakdown of how many targets are observed in each sector.

While the CTL includes a great deal of curation, it is not infallible. A particular weakness inherent to stellar catalogs based on photometric colors is in distinguishing between dwarf stars and subgiants (Huber et al. 2014; Mathur et al. 2017). CTL versions up through 6.2 use parallax information when available to determine stellar radii (and therefore luminosity class), but the vast majority of stars depend on the use of RPM cuts to distinguish dwarfs from giants. While *GAIA* DR2 will shortly provide reliable parallaxes for most CTL stars (Davenport 2017; Huber et al. 2017; Stassun et al. 2018), the CTL will not be significantly modified until 2019. Furthermore, while the RPM method is highly reliable at distinguishing dwarfs and subgiants as a group from giant stars, it is generally not useful for distinguishing dwarfs from subgiants. Of the CTL stars that are classified as dwarfs based on the RPM cut, about 40% are actually subgiants, although roughly 35% of the CTL stars have parallax measurements confirming their spectral class. To account for this effect, we simulated a misclassified population of subgiants by increasing the stellar radius of 40% of those AFGK stars that had been selected with the RPM cut by a factor of 2, with the affected stars drawn at random. That included 25% of all the AFGK stars in the CTL. This approach somewhat overestimates the radii of A-type subgiants, but the effect on total planet yield is limited, because A-type stars have large radii, making detecting transiting planets challenging, and thus are already a relatively small fraction of the high-priority CTL stars.

2.2. Simulating Planets

To each star in our list we assigned zero or more planets. The number of planets assigned to each star was drawn from a Poisson distribution. The mean (referred to here as λ) of the Poisson distribution we used differs between AFGK dwarf stars and M dwarfs because there is strong evidence that M dwarfs host more planets on short orbital periods (Burke et al. 2015; Mulders et al. 2015). For AFGK stars we used the average number of planets per star with orbital periods of up to 85 days of $\lambda = 0.689$ (Fressin et al. 2013), while for M stars $\lambda = 2.5$ planets are reported with orbital periods up to 200 days (Dressing & Charbonneau 2015).

Each planet was then assigned six physical properties drawn at random: an orbital period (P), a radius (R_p), an eccentricity, a periastron angle, an inclination to our line of sight (i), and a midtime of first transit. The orbital period and radius were selected using the exoplanet occurrence rate estimate of Fressin et al. (2013) for AFGK stars and Dressing & Charbonneau (2015) for M stars. Both Fressin et al. (2013) and Dressing & Charbonneau (2015) reported occurrence rates in period/radius bins. We drew at random from each of these bins with the probability to draw from a given bin weighted by the occurrence rate in that bin divided by the total occurrence rate of planets. For example, Dressing & Charbonneau (2015) reported a 4.3% occurrence rate for planets with radii 1.25–2.0 $R_\oplus$ and orbital period 10–17 days, so in our simulation we drew planets from that bin with a frequency of 4.3 divided by the total occurrence rate in all bins. We normalized by the total occurrence rate of planets since we already took account of systems with zero or multiple planets in the Poisson draw. Once we knew which bin to select a planet from, we drew from a uniform distribution over the bin area to select an orbital period–radius pair, except for the giant-planet bin where we draw from a power-law distribution in planet radius with exponent -1.7, which mirrors Sullivan et al. (2015). This nonuniform giant-planet size distribution reduces the number of nonphysical inflated planets, as discussed by Mayorga & Thorngren (2018). Occurrence rates from both Fressin et al. (2013) and Dressing & Charbonneau (2015) are based on *Kepler* data and are limited in orbital period to 0.5–85 days and 0.5–200 days, respectively.

Following Kipping (2014), the orbital eccentricity was selected from a Beta distribution, with parameters $\alpha = 1.03$ and $\beta = 13.6$, which Van Eylen & Albrecht (2015) found were appropriate for transiting planets. The periastron angle was drawn from a uniform distribution between $-\pi$ and $+\pi$. The cosine of inclination was chosen to be uniform between zero and one. Planets in multiple-planet systems were assumed to be coplanar—i.e., they have the same cos i—which is a reasonable assumption because multiple-exoplanet systems have been found to be highly coplanar (Xie et al. 2016). Finally, we chose a time of first transit to be uniform between zero and the orbital period—note that this may be greater than the total observation duration, in which case no transit was recorded. We then computed the number of transits observed using the observation duration calculated previously (the number of sectors where a target is observed).

We intentionally kept planets that cross the orbit of other planets in the system because, while they are likely on unphysical orbits, to remove them would change the distribution of the number of planets per star, which is an observed property. We also assumed that none of these planets experience a significant amount of transit timing variations (S. Hadden et al. 2018, in preparation, address transit timing variations and period ratios in detail).

2.3. Detection Model

Armed with a sample of planets and host stars, we then determined which planets are detectable. To do this, we derived a transit depth modified by several factors: the flux contamination of nearby stars, the number of transits, and the transit duration. It should be noted that flux contamination is significantly more problematic for *TESS* than with *Kepler* because *TESS* has pixels that are 28 times larger than *Kepler*'s.

The raw transit depth was computed assuming a uniform disk (i.e., transit depth $T_d = (R_p/R_\star)^2$, where $R_\star$ is the stellar radius). That is, we ignored the effects of limb darkening and grazing transits. We calculated the reduction in transit depth due to dilution from nearby stars using the value of contamination for the CTL as $T_d/(1+d)$, where d is the dilution, the fraction of light coming from stars that are not the target divided by the total star light. We then multiplied the transit depth by the square root of the transit duration ($T_{\rm dur}$) in

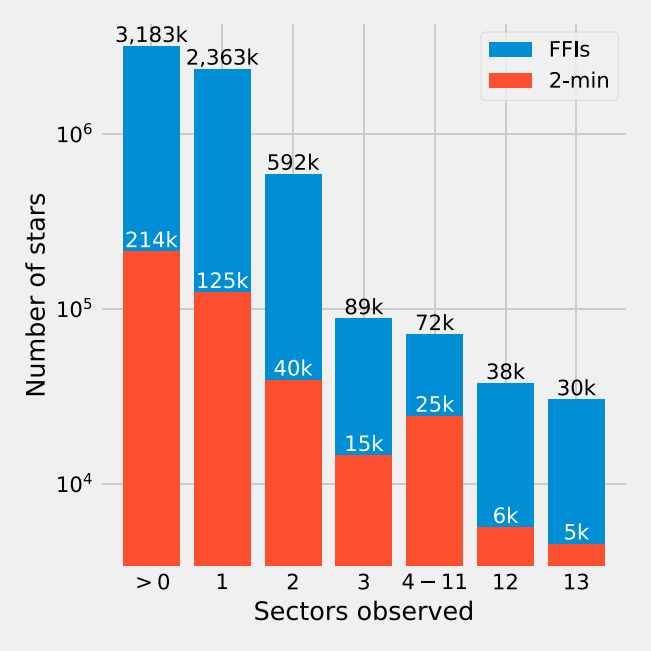

Figure 2. Number of CTL targets observed for a given number of 27.4-day sectors. FFI targets are shown in blue, and 2-minute cadence targets in red. In total, 3.2 million CTL targets are observed, of which 214,000 are observed at 2-minute cadence. Roughly three-quarters of targets are only observed for a single sector, with just 2.1% having 12 or 13 sectors of coverage. The 2-minute cadence targets are disproportionately observed for more sectors, with 4.2% of the 2-minute cadence targets receiving 12 or 13 sectors of coverage.

hours, with transit duration following Winn (2010) defined as

$$T_{\rm dur} = \frac{P}{\pi}\arcsin\left[\frac{R_\star}{a}\frac{\sqrt{(1+R_p/R_\star)-b^2}}{\sqrt{1-\cos^2 i}}\right], \quad (1)$$

where P is the orbital period, i is the orbital inclination relative to our line of sight, $a/R_\star$ is the semimajor axis in units of stellar radius, b is the impact parameter, and $R_p/R_\star$ is the planet-to-star radius ratio, to derive an effective transit depth. The effective transit depth, T_d', is defined as

$$T_d' = (R_p/R_\star)^2 \times \sqrt{T_{\rm dur}} \times \sqrt{N} \times \frac{1}{1+d}, \quad (2)$$

where N is the number of transits observed.

We took the *TESS* photometric noise level from Stassun et al. (2017), who used the properties described by Ricker et al. (2016) and tested whether the effective transit depth was greater than the *TESS* photometric noise at the stellar brightness of the host stars multiplied by 7.3 (i.e., signal-to-noise ratio $[S/N] \geqslant 7.3$). A 7.3σ detection is the nominal value used by Sullivan et al. (2015) and is calculated in a similar manner to the detection threshold used by *Kepler* (Jenkins et al. 2010). We also required that the impact parameter of the transit is less than 1.0 and that we observed at least two transits. Requiring an impact parameter of less than 1 removes a small number of grazing transits, but these are difficult to distinguish from eclipsing binaries anyway (Armstrong et al. 2017). These detection thresholds are relatively aggressive; Section 4.2 describes using more conservative detection thresholds of at least three transits and S/N of 10.

3. Results

We performed 300 simulations using our nominal planet sample and detection criteria; this enabled us to look at the average and range from our simulations. We predict that *TESS* will find 4373 planets (median) orbiting stars on the CTL, with the 90% confidence interval ranging from 4260 to 4510 planets. Henceforth, we designate a simulation that produced the median number of planets as our fiducial simulation, and the properties we show come from that simulation. All the stars in the CTL are included in Figure 3, and the detected planets are shown as red circles.

Our fiducial simulation has 1293 planets orbiting 2-minute cadence targets, and the 90% confidence range of planets found in 2-minute data is 1180–1310 planets. The sky distribution is shown in Figure 4. There are clear differences in features between the FFI distributions and the 2-minute cadence distributions. The FFI stars are not evenly distributed; there is a lower density of stars in the southern sky. This is caused by the use of the RPM cut to identify dwarf stars, since existing proper-motion catalogs are less complete below a declination of $-30°$. This low density at southern latitudes is not visible in the 2-minute cadence plots because the high-quality AFGK stars chosen for 2-minute cadence observations are bright enough that the proper-motion catalogs are essentially complete for them. However, M dwarfs are faint enough that the proper-motion catalogs are not complete for even high-priority stars below a declination of $-30°$, and they are undersampled among the 2-minute targets in that region.

The Galactic plane is visibly underpopulated in the 2-minute cadence data for two related reasons. Stars near the Galactic plane tend to have higher flux contamination, which depressed their calculated priority. Also, photometric catalogs have a great deal of unreliability in the Galactic plane in variety of ways, including proper motions, source identification, and the effects of reddening on the stellar temperatures. Therefore, the priorities of all CTL stars within 15° of the Galactic plane were systematically down-weighted in the CTL, except for a subset of specially identified stars.

For both the 2-minute and the FFI-observed stars, we found planets more frequently closer to the ecliptic poles, where the longer observing baseline makes transit detection easier and where it is possible to find longer-period planets.

As shown in Figure 5, our simulation predicts that *TESS* will find 41 Earth-sized worlds ($<1.25\,R_\oplus$), 238 super-Earths (1.25–$2.0\,R_\oplus$), 1872 sub-Neptunes (2.0–$4.0\,R_\oplus$), and 2222 giant planets ($>4.0\,R_\oplus$) orbiting stars on the CTL. In total, 279 planets smaller than $2.0\,R_\oplus$ were detected in our simulation, 90% of which were orbiting targets observed at 2-minute cadence. The sub-Neptunes were split roughly evenly between those observed at 2-minute cadence and those found only in FFI data, but nearly 90% of giant planets were found in the FFI data.

A summary of the properties of planets detected in FFIs and 2-minute cadence data is given in Table 1. Full details of every planet detection in our simulation are provided in a machine-readable table, with a summary shown in Table 2.

About 75% of stars were observed for a single sector. Unsurprisingly, most planets (2334%, 53%) were also only observed for a single sector, and three-quarters of planets were observed for one or two sectors. Conversely, while just 2% of CTL stars were observed for 12 or 13 sectors, 11% of all planets detected were found around these stars. The number of

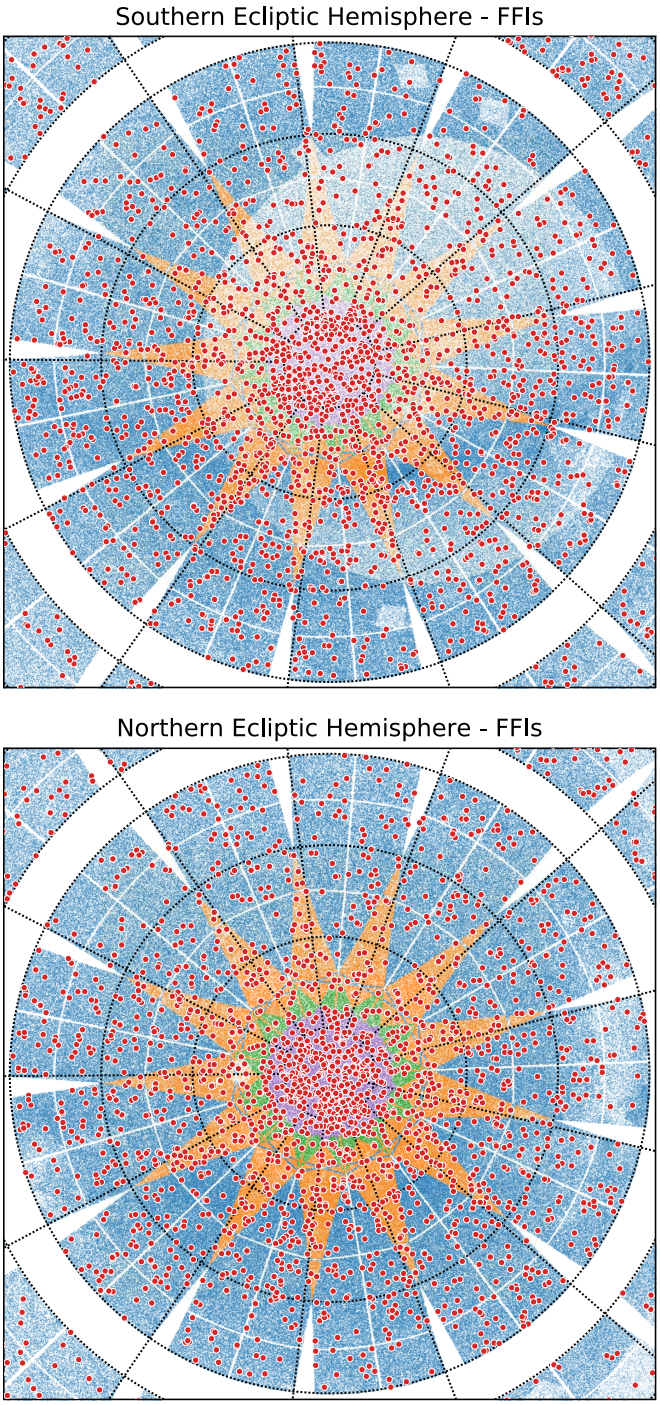

Figure 3. Spatial distribution of target stars and detected planets from FFI data. The top panel shows the southern ecliptic hemisphere, and the bottom panel shows the northern ecliptic hemisphere. Stars observed for one sector are shown in blue, two sectors in orange, three or more sectors in green, and stars in the CVZ are shown in purple. Detected planets are shown as red circles. A total of 4373 planets are shown, of which 54% were only observed for a single sector, and 11% were observed for 12 or 13 sectors. The lower density of stars, offset from the south ecliptic pole, is centered on the south celestial pole and is due to relatively incomplete proper-motion catalogs in the celestial south.

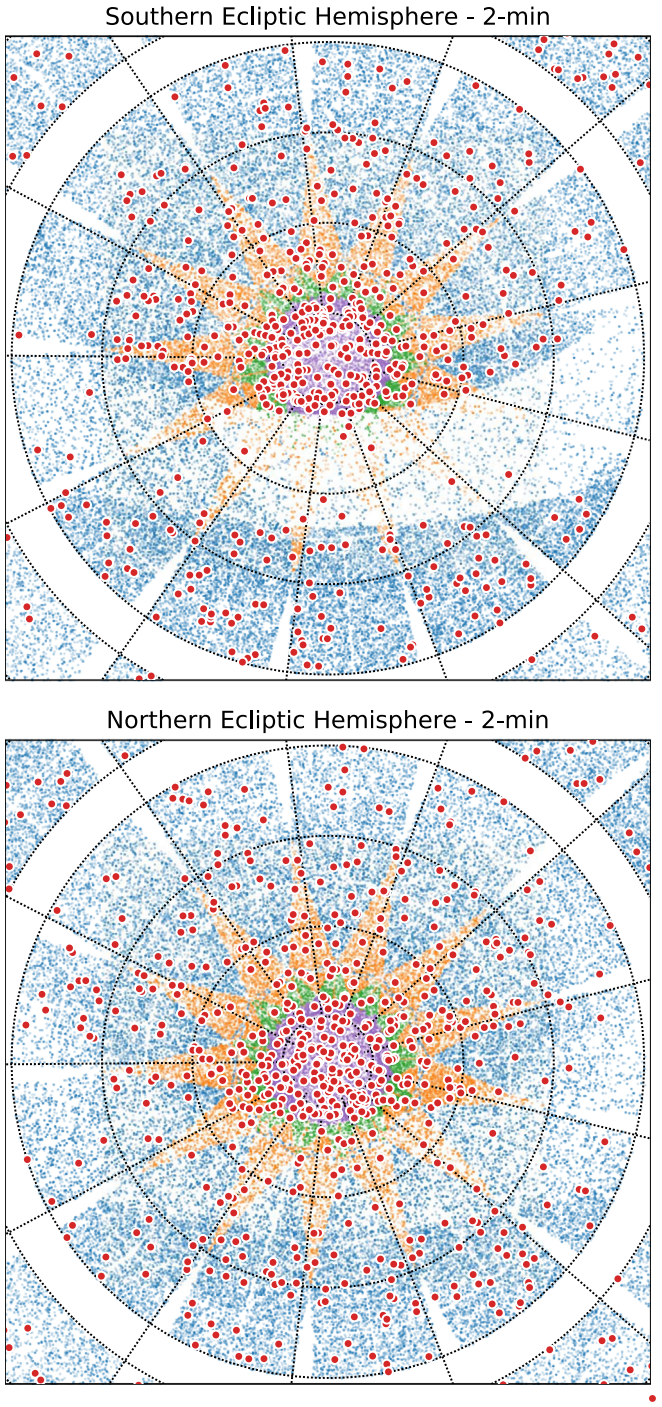

Figure 4. Spatial distribution of target stars and detected planets from 2-minute cadence data. The colors of stars and planets are the same as shown in Figure 3. The southern hemisphere, and to a lesser extent the northern hemisphere, has a pronounced feature of the Galactic plane running through where priorities are down-weighted because the high stellar density will dilute transit signals, making them harder to detect.

sectors that a planet is observed for is shown in Figure 6. The longer observing baseline gave both higher-S/N transits and sensitivity to longer orbital period planets. The number of stars observed at 2-minute cadence for 12 or 13 sectors was fairly heavily constrained in our target selection model; therefore, a relatively high fraction (60%) of planets were found in the FFI data for the high-latitude fields. Overall 70% of planets were found only in the FFIs, but for stars that were observed between 4 and 11 sectors, just 40% of planets were found only in the FFI data.

The orbital periods of our planets ranged from 0.5 to 99 days, which is a somewhat artificial limitation based on the occurrence rates used. The minimum orbital period of the injected transit signals was 0.5 days. While we know of several ultrashort-period planets (e.g., Sanchis-Ojeda et al. 2013), they

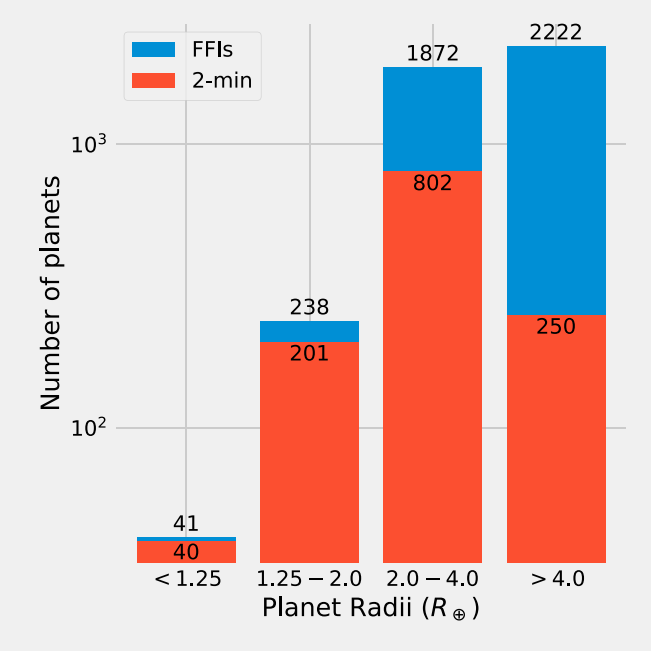

Figure 5. Our simulations predict that *TESS* will detect a total of about 4400 planets orbiting stars on the CTL, of which 1300 will be observed at 2-minute cadence. Roughly 40 Earth-sized planets will be found, almost all of which are on the 2-minute target list. A total of 1000 super-Earths and mini-Neptunes will also be found. Many new giant planets will be discovered, primarily through FFI data. The numbers shown above the FFI bars are total planets and include the planets found in 2-minute cadence data.

are very rare (Winn et al. 2018) and therefore will not significantly impact the planet yield. On the long-period end, we simulated M dwarf planets with periods up to 200 days, yet no planets with periods longer than 100 days were recovered, so we are confident that few long-period planets were missing here. For hotter stars, we only simulated planets with periods up to 85 days. It is likely we were missing planets orbiting stars with periods longer than 85 days. However, we only found two planets in our M dwarf sample with periods longer than 85 days, and in the period range of 65–85 days for the AFGK sample we had just 17 planets. Since the probability of a planet to transit scales inversely with orbital distance, and the number of stars with a long enough observing baseline to detect at least two transits similarly shrinks, we do not expect more than a handful of additional long-period planets. We do caution that our sample should probably not be used to estimate the yield of planets showing a single transit because the 85-day limit becomes more significant. For a study of single transiting planets we point readers to Villanueva et al. (2018).

In Figure 7 we show the ratio of stars observed to planets detected—which we define as the "hit rate." Overall, the hit rate for 2-minute cadence targets was 0.60%, while for the CTL stars not on the 2-minute cadence list the hit rate was 0.10%. Hit rate increases with observing duration, from 0.43% for 2-minute cadence targets observed for one sector up to 1.8% for 2-minute cadence targets with at least 12 sectors of data.

We found that the planet host stars range in brightness from *V*-band mag of 4.0 to 20, with seven planets predicted to orbit stars brighter than 55 Cnc, currently the brightest transiting planet host (Winn et al. 2011). As shown in Figure 8, in the *TESS* bandpass, 90% of planets orbited stars with magnitudes between 8.2 and 13.1, compared with $Kp = 11.9$–15.9 for *Kepler* planet candidates (Thompson et al. 2018). The simulated planets typically orbited stars 3 mag brighter than *Kepler* planets. Planets around stars observed at 2-minute cadence were systematically brighter than the planets found orbiting stars observed only in FFI data, with a median *TESS* magnitude of 10.4 versus 11.0.

With *TESS* concentrating on finding planets orbiting cool stars, it is unsurprising that many planets orbited stars that were bright in the infrared. The median K_s-band ($\sim$2.0–2.2 μm) magnitude of planets in 2-minute cadence data was 9.2, and 90% of 2-minute cadence planets were brighter than $K_s = 10.7$. None of the *TESS* 2-minute planets orbited stars fainter than the median infrared brightness of *Kepler* planet candidates of $K_s = 13.0$.

The spectral type distribution of the detected planet host stars is shown in Figure 9. About one-quarter of the planets found in 2-minute cadence data orbited M dwarfs (371), with the remaining split fairly evenly between K (216), G (351), and F (299) stars. The deficit in planets orbiting K dwarfs was caused by a deficit in K dwarfs selected for 2-minute cadence observations. This was a result of the target prioritization strategy employed and has been noted previously (Stassun et al. 2017). A few additional planets orbiting cool stars were found in FFI data (only 125 additional M dwarfs), but 80% of FFI-only planets orbited stars larger than the Sun. In total, about 10% of planets in our simulated sample orbited M dwarfs.

Figure 10 shows the distance to the simulated planets.[5] The closest detected planet in our simulation orbited Lalande 21185, a star 2.5 pc away. We found 46 planets within 50 pc and 234 planets within 100 pc, which doubles and quadruples the number of transiting planets known within 50 and 100 pc, respectively (Akeson et al. 2013).

The circumstellar habitable zone concept has been popular since at least the 1950s (Shapley 1953; Strughold 1953) and refers to the spherical shell around a star where liquid water could be present on a planetary surface. Kopparapu et al. (2013) provided models for an optimistic habitable zone with boundaries of recent Venus and early Mars, which correspond to stellar fluxes of 1.78× and 0.32× the insolation Earth receives from the Sun, respectively. Our simulation contains 69 planets in the optimistic zone, of which 9 are smaller than 2 $R_\oplus$. All the habitable zone planets orbit M dwarfs.

3.1. Suitable Targets for RV Follow-up

For the *TESS* mission to be successful, it must find planets smaller than 4 $R_\oplus$ with a measurable RV signal. We predict that *TESS* will find more than 2100 planets smaller than 4 $R_\oplus$, but many of these will orbit stars whose brightness makes follow-up challenging or impossible with current-precision RV facilities. While planets orbiting very faint stars have had their mass determined via RV studies (e.g., Koppenhoefer et al. 2013), it is typically challenging to measure masses of planets around stars fainter than $V = 12$. We predict that *TESS* will find 1300 planets smaller than 4 $R_\oplus$ around stars brighter than $V = 12$. Therefore, with more than 1000 potential targets, *TESS* will have a plethora of targets to choose from when selecting promising RV targets. Even if just 20% are good RV

[5] Only about half of the targets in our sample had distances reported in CTL version 6.1; our statistics are based on this sample. Furthermore, a small number of the CTL-reported distances were unrealistically large. These issues have been fixed in CTL v6.2.

Table 1
Summary of the Properties of the Planets Detected in Our Fiducial Simulation

	2-minute Cadence			FFIs		
Property	Median	5th Percentile	95th Percentile	Median	5th Percentile	95th Percentile
Host star radius ($R_\odot$)	1.02	0.23	2.44	1.35	0.32	3.48
Host star mass ($M_\odot$)	0.95	0.20	1.61	1.07	0.32	1.93
Host star temperature (K)	5500	3200	7200	5900	3400	8000
Host star brightness, K_s	9.2	6.7	11.0	10.0	7.4	11.5
Host star brightness, *TESS* mag	10.4	7.5	13.5	11.0	8.2	13.1
Host star brightness, V	11.3	7.9	16.3	11.7	8.8	15.4
Planet radius ($R_\oplus$)	3.1	1.4	8.9	4.2	1.9	15.1
Planet orbital period (days)	8.2	1.7	34.8	7.0	1.8	29.0
Transit duration (hr)	3.0	1.0	8.7	3.9	1.3	10.4
S/N	13.6	7.7	109	13.3	7.6	93.7
Number of transits	7	2	65	6	2	51
Distance (pc)	140	50	200	260	70	890

Note. The FFI results include planets also found in the 2-minute cadence data.

targets, this will more than triple the number of planets smaller than 4 $R_\oplus$ with measured masses.

There are 160 planets in our sample that are smaller than 2 $R_\oplus$ and orbit stars brighter than $V = 12$. We currently have mass and radius constraints on fewer than 60 planets smaller than 2 $R_\oplus$, so *TESS* will potentially greatly increase this number, although the precise number will depend on whether individual stars are suitable for precise RV measurements.

3.2. Targets for Atmospheric Characterization

A second aim of the *TESS* mission is to find targets suitable for transmission spectroscopy using *JWST*. Until on-sky performance is measured, particularly the systematic noise level, there is considerable uncertainty on how *JWST* will perform (Batalha et al. 2017). However, we can identify the properties of planets that would make them good *JWST* targets using a few simple cuts. The host star should be bright in the infrared, and the star should be small. We identified simulated planets whose host stars have $K_s < 10$, $T_{\rm eff} < 3410$ K, which equates to M3V stars with a radius of approximately 0.37 solar radii (Pecaut & Mamajek 2013). In total, there were 70 planets fulfilling these criteria. We show in Figure 11 the simulated small planets we think make interesting candidate *JWST* targets in terms of insolation fluxes. There are 10 planets in the boxed region in Figure 11, which highlights planets that fell into the optimistic habitable zone (Kopparapu et al. 2013) and had radii between 1.25 and 2.5 $R_\oplus$, implying a puffed-up atmosphere (Lopez & Fortney 2014). These planets, along with those orbiting TRAPPIST-1 (Gillon et al. 2017) and other low-mass stars (Greene et al. 2016; Kreidberg & Loeb 2016; Morley et al. 2017; Louie et al. 2018), will form a reference sample of temperate worlds for observation by *JWST*.

The *JWST* CVZ is located within 5° of the ecliptic poles and is contained within the *TESS* CVZ, shown in Figure 1. However, because of gaps between the *TESS* CCDs on Camera 4 (each camera is composed of a 2 × 2 grid of CCDs), the central 2° has limited coverage. In our sample we have 74 planets with ecliptic latitude $|b| > 85°$, of which 29 are 2-minute cadence targets and 11 are smaller than 2 $R_\oplus$.

4. Discussion

4.1. Alternative Selection Strategies for the 2-minute Cadence Targets

In addition to the nominal 2-minute cadence target selection laid out in Section 2.1, we also considered alternative strategies of selecting a higher or lower fraction of targets in the CVZ, which we call scenarios (a) and (b), respectively. There are justifications for both approaches. Placing more of the 2-minute cadence targets in the CVZ increases the overall number of 2-minute targets where *TESS* is sensitive to long-period planets, and potentially to smaller planets via increased S/N. On the other hand, placing more of the 2-minute targets outside the CVZ should increase the overall number of planets detected, since 13 stars can be observed in regions with single-sector coverage for each target in the CVZ.

To test these scenarios, we selected targets in an identical manner to that described in Section 2.1, except that in scenario (a) we included 12,000 stars in the CVZ and 2200 stars in the other cameras per sector, while in scenario (b) we select 3000 CVZ targets and 11,200 stars in the remaining cameras.

Under these two different selection strategies, we examined the number of planets found in 2-minute cadence data, compared to our nominal selection strategy. In scenario (a) we found a total of 740 ± 50 planets, and in scenario (b) we found 1380 ± 60 planets, which compares with 1250 ± 70 planets in the nominal strategy (where the reported value is the median, and uncertainties are the central 90% of the distribution, calculated by 300 Monte Carlo simulations). These results suggest that the nominal selection strategy was reasonably successful at accomplishing the goal of maximizing the number of planets with 2-minute cadence photometry, which in turn maximizes the number of planets where we can derive precise stellar parameters through asteroseismology (Campante et al. 2016). Scenario (b) yielded 10% more planets, but the results were comparable within uncertainties, and the number of planets with orbital periods beyond 15 days was cut by about 10% in scenario (b). Scenario (a) extended the tail of the orbital period distribution—the 95th percentile shifts from 30 to 42 days—but because of the large decrease in the total number of planets, the absolute number of long-period planets was unchanged.

Table 2
Planet and Host Star Properties for Every Detected Planet in Our Simulation

Num	Units	Label	Explanation
1	⋯	TICID	*TESS* Input Catalog ID number of star
2	deg	RAdeg	R.A. 2000
3	deg	DEdeg	Decl. 2000
4	deg	ELON	Ecliptic longitude
5	deg	ELAT	Ecliptic latitude
6	⋯	Priority	CTL v6.1 priority
7	⋯	2min-target	Was this a 2-minute cadence target in our model? 1 = yes, 0 = no
8	⋯	Camera	*TESS* camera number, number between 1 and 4
9	d	Obslen	Number of days that target is observed
10	⋯	Num-sectors	Number of sectors the target is observed for
11	mag	Vmag	*V*-band magnitude
12	mag	Kmag	K_s-band magnitude
13	mag	Jmag	*J*-band magnitude
14	mag	Tmag	*TESS* bandpass magnitude
15	solRad	Star–radius	Stellar radius
16	solMass	Star–mass	Stellar mass
17	K	Star-teff	Stellar effecitve temperature
18	pc	Distance	Distance of the star
19	⋯	Subgiant	Was this star randomly selected to be a subgiant? 1 = yes, 0 = no
20	⋯	Detected	Was this planet detected? 1 = yes, 0 = no
21	⋯	Detected-cons	Was this planet detected using the conservative model? 1 = yes, 0 = no
22	day	Planet-period	Orbital period of the planet
23	Rgeo	Planet-radius	Radius of the planet
24	⋯	Ntransits	Number of transits the planet has, 0 if planet does not transit
25	⋯	Ars	Planet semimajor axis divided by the stellar radius
26	⋯	Ecc	Planet orbital eccentricity
27	⋯	Rprs	Planet radius divided by the stellar radius
28	⋯	Impact	Planet impact parameter
29	hr	Duration	Planet transit duration
30	ppm	Depth-obs	The observed transit depth, corrected for dilution
31	⋯	Insol	Insolation flux the planet receives relative to that received by the Earth from the Sun
32	ppm	Noise-level	The 1 hr integrated noise level of the star
33	⋯	S/N	Combined signal-to-noise ratio of all transits, 0 if planet does not transit

(This table is available in its entirety in machine-readable form.)

In each scenario the total number of planets detected remained unchanged because almost all planets could be found equally well in 2-minute cadence and FFI data, so the precise stellar selection had limited impact on the primary mission goals.

4.2. A More Conservative Model

Our analysis so far has made two fairly optimistic assumptions: (1) that we can identify a transiting planet by observing just two transits from *TESS*, and (2) that we can detect all planets with an S/N $\geqslant$ 7.3. In actuality, planets with fewer than three observed transits are very difficult to uniquely

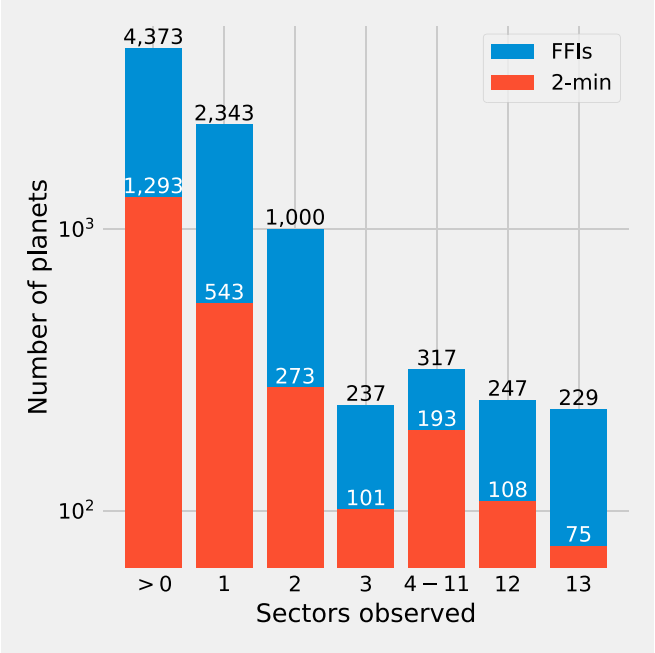

Figure 6. Number of sectors that stars with detected planets were observed for, with a sector having an average observing window of 27.4 days. More than half of planets were observed for a single sector, with 10% being observed for 12 or 13 sectors.

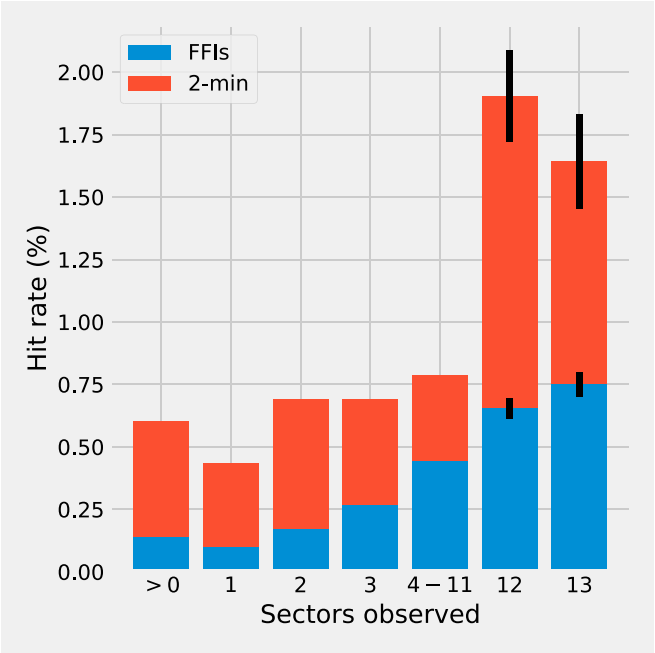

Figure 7. Ratio of stars observed to planets detected as a function of the number of sectors a star is observed for. The longer a star was observed, the higher probability a planet would be detected. Targets observed at 2-minute cadence are shown in red, while blue are FFI targets. For 2-minute cadence stars the average hit rate was 0.60%, while including all stars on the CTL drops this to 0.14%. While observing for a longer baseline increased the number of planets, the increase is not linear. For 2-minute cadence targets, an increase of 12× in observing baseline increased the hit rate by a factor of just 4.4. There are comparatively few planets in the 12 and 13 sector bins, so we show Poisson uncertainties on these bars demonstrating that there is not a measurable difference between observing for 12 or 13 sectors. Red and blue bars are not stacked; both start at zero.

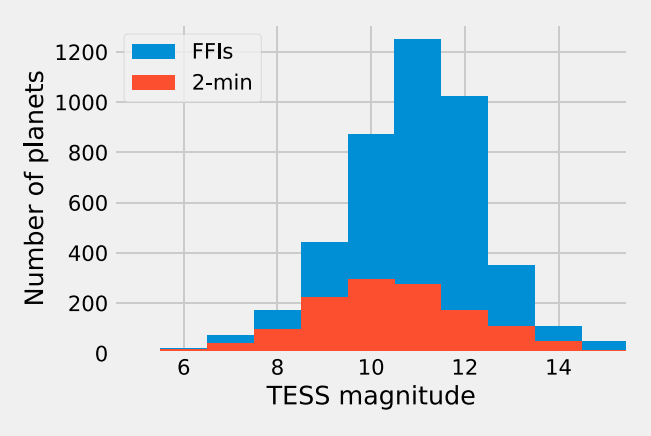

Figure 8. Brightness of the planet host stars in the *TESS* bandpass magnitude. The median brightness of stars with planets found in 2-minute cadence data was 10.4, with a maximum range of 3.5–15.3. For planets found only in FFI data, the median brightness was 11.3, with a maximum range of 6.1–16.4.

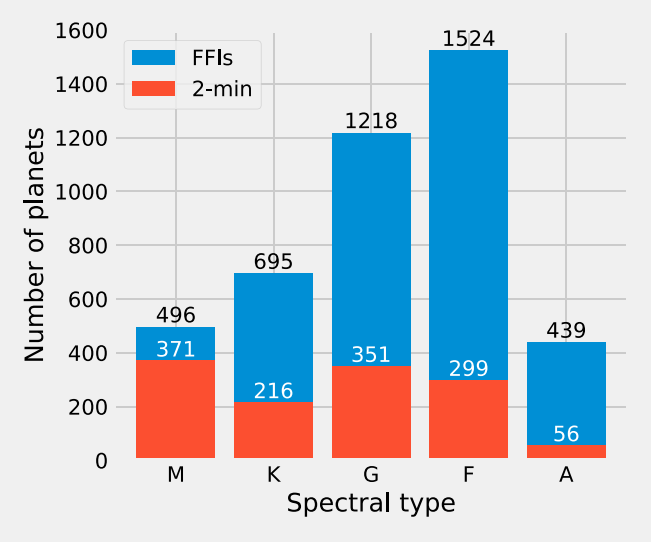

Figure 9. Spectral type distribution of *TESS* planet-hosting stars. Our simulations predict that *TESS* will find 496 planets orbiting M dwarfs, of which 371 orbit stars were observed at 2-minute cadence. About half the simulated planets in 2-minute cadence data orbited stars larger than the Sun, while 80% of planets found only in FFI data orbited stars larger than the Sun.

identify using photometric survey data alone (see Mullally et al. 2018; Thompson et al. 2018). Planets have been detected using *K2* mission data (Howell et al. 2014) with one (Vanderburg et al. 2015) and two (Crossfield et al. 2015) transits, but these cases occurred in systems where additional space-based follow-up assets were exploited or there were two other planets in the system, so the validity of the planets was less ambiguous (Lissauer et al. 2012). While with sufficient observing resources characterizing these planets is feasible, they remain a challenge. Furthermore, analyses of *Kepler* data have shown that using a detection threshold below 8σ–10σ leads to many spurious detections (Christiansen et al. 2016; Mullally et al. 2018; Thompson et al. 2018). In *K2*, a threshold of $S/N > 12$ was typically applied (Crossfield et al. 2016) before expending follow-up resources on a candidate planet.

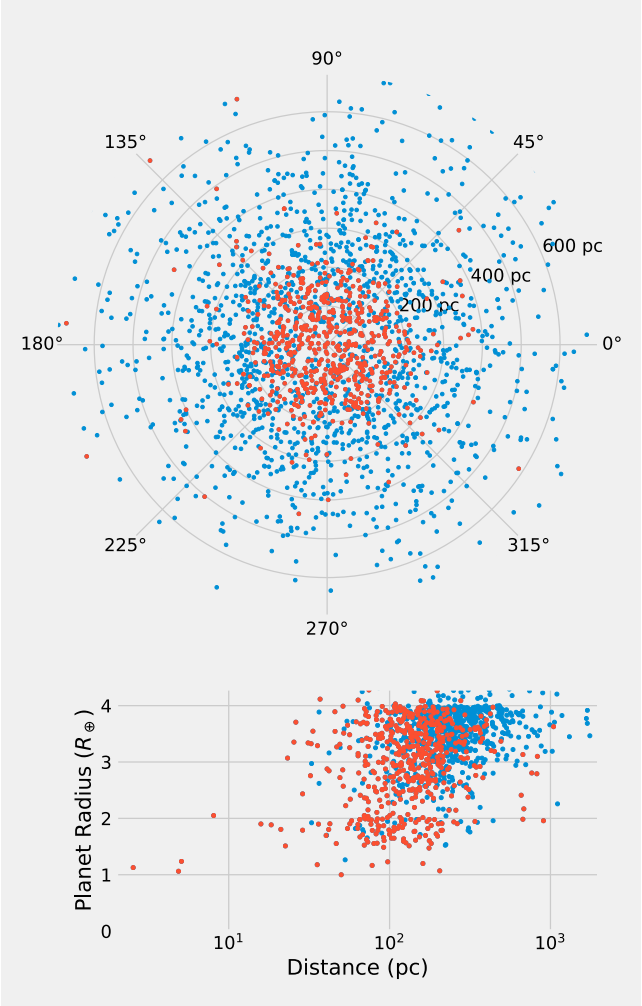

Figure 10. Distances of planets found in our simulation in parsecs. The top panel shows both distance and ecliptic latitude of the host stars, and the bottom panel is distance plotted against planet radius. Almost all 2-minute cadence planets discovered by *TESS* will be within 300 pc, with 77% within 200 pc. FFI planets were found over 1000 pc away, but 90% of planets were within 700 pc.

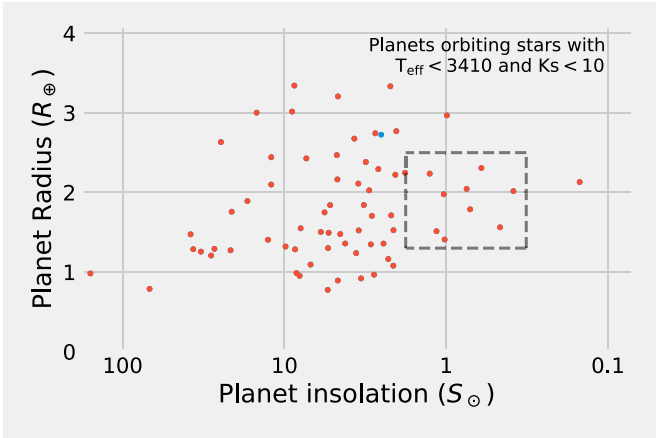

Figure 11. Planets make good targets for transmission spectroscopy if they orbit bright, small stars. This plot shows planets that orbit stars with spectral type M3V or later and that are brighter than $K_s = 10$. The box is an approximate region showing planets that may have somewhat extended atmospheres (i.e., super-Earths) and are in the circumstellar habitable zone. There are 10 planets within this region, making up the prime *JWST* target sample from *TESS*.

With these limits in mind, we took the fiducial catalog and cut planets that either had fewer than three transits or had a combined transit S/N < 10. This resulted in a moderate cut in the total number of planets found to 2609 total planets, of which 820 came from the 2-minute cadence data. This was a 60% overall decrease in the total number of planets detected, but it was most significant for small planets. The number of planets with radii below 2 $R_\oplus$ decreased by a factor of two from 279 to 128 planets, with similar fractional losses in the 2–4 $R_\oplus$ bin, but there was only a 25% decrease in detected giant planets. Figure 12 shows the size distribution of planets found under the conservative detection model.

The decrease in the number of planets amenable to RV follow-up was roughly a factor of two, with planets smaller than 4 $R_\oplus$ orbiting stars with $V < 12$ dropping from 1312 to 616, and those smaller than 2 $R_\oplus$ from 151 to 67. The number of habitable zone planets dropped from 69 to 28 and left just four smaller than 2 $R_\oplus$. The number of premium *JWST* targets sees a modest decrease. The number of planets orbiting stars cooler than 3410 K, with $K_s < 10$, drops from 71 to 58, and the number in the dashed box in Figure 11 dropped from 10 to 7. While these drops were significant, they are unlikely to seriously impact the primary mission goal, because there were still hundreds of small planets orbiting bright stars in the sample.

4.3. Phantom Inflated Planets

This study and other planet yield simulations (e.g., Sullivan et al. 2015) have not paid particular attention to the physical properties of giant planets, primarily because these are not a focus for the *TESS* mission team. Nevertheless, we are anticipating groundbreaking scientific advances in our understanding of the atmospheres of giant planets from follow-up observations of planets found by *TESS*—particularly from *Spitzer*, *Hubble Space Telescope*, and *JWST*. As pointed out by Mayorga & Thorngren (2018), in the first version of this paper there were significant numbers of giant planets that were beyond the limit of inflation for their equilibrium temperatures (Thorngren & Fortney 2018). The cause of this is that in the occurrence rate estimates of Fressin et al. (2013) the giant-planet bin spans 6–22 $R_\oplus$ while temperate planets should rarely be larger than 12 $R_\oplus$. As a result of this feedback from Mayorga & Thorngren (2018), we changed the selection function in the giant-planet bins from a lognormal function to a power law. This reduced the number of phantom planets from 8% of the total population to 1%. We caution giant-planet aficionados that there are 45 overinflated giant planets in our simulation.

4.4. The Effects of Earth and Moon Crossings

The nature of the *TESS* orbit means that a subset of observations will be obscured by the Earth or Moon passing through the field of view. Cameras that receive a significant amount of scattered light from the Earth or Moon will experience larger background flux, and photometry in any camera that receives a large portion of direct light from the Earth or Moon will likely be impossible because of saturation and bleed. However, the Earth and Moon move relatively quickly through the field of view, and Earth or Moon crossings are relatively infrequent (Ricker et al. 2015). Bouma et al. (2017) estimated that the Earth and Moon will significantly affect photometric performance for 9% of all exposures, although the lost cadences will not be evenly distributed in time or focal plane location. Camera 1 and, to a lesser degree, Camera 2 are impacted, but the effect was expected to be limited for Cameras 3 and 4. Estimating how this affects the yield is nontrivial, but we can try by using the Bouma et al. estimates that 23% of observations in Camera 1 and 12% of observations in Camera 2 will be affected. We can then assume that the S/N of transits will scale with the square root of the number of observations, so Camera 1 targets will have 11% lower S/N, and Camera 2 targets will have 6% lower S/N. This causes a 13% drop in total planets detected in our simulation and a 9% decrease in the number of planets orbiting 2-minute cadence targets. Early commissioning results have suggested that the effect of the Moon may be more complex than anticipated, and owing to the substantial uncertainty in the impact of Earth and Moon crossings, we have not included Earth and Moon crossings in our yield statistics.

4.5. Astrophysical False Positives

Sullivan et al. (2015) performed a careful analysis of the sources and rates of false positives expected in the *TESS* 2-minute cadence data, and we have not reproduced that work here. They estimated that *TESS* will find over 1000 astrophysical false positives in 2-minute cadence data, but they described promising mitigation strategies that utilize follow-up observations and statistical methods to reduce this by a factor of 4 or more.

The ratio of false positives to detected planets will not be uniform over all stars observed by *TESS*, but it will vary as a function of hit rate. In Section 3 we showed that the hit rate for 2-minute cadence targets is a factor of 5.5 higher than FFI-only stars. Assuming that each star has the same chance of yielding a detection of an astrophysical false positive, the fraction of true planets found to false positives will be lower for the FFI-only detections than for 2-minute cadence targets. The reason is that fewer planets are found per stars observed but the same number of false positives are detected. Using the false-positive rate from Sullivan et al. (2015) of 1 false positive per 180 stars observed yields one astrophysical false positive per planet detection. However, for the FFI-only targets the ratio of false positives to planets detected increases to more than five per true planet discovered.

Furthermore, stars on the CTL that are not included in our 2-minute cadence sample are, on average, 2 mag fainter than the 200,000 stars observed at 2-minute cadence. This means that mitigation strategies that rely on follow-up observations will be significantly more challenging. Given that essentially all small planets will be found in the 2-minute cadence data, only the most intrepid of exoplaneteers will want to commit significant resources to discovering and following up planets in FFI data.

4.6. Planets Detected around Stars Not in the CTL

In Section 2.1 we simulated planets orbiting stars that are in CTL version 6.1. This totals roughly 3.2 million stars but includes only those stars that the *TESS* Target Selection Working Group considered as potential 2-minute cadence

targets. The limited number of slots available for 2-minute cadence requires not just a careful consideration of the overall potential for planet detections around a given star but also comparison of the relative planet detection potential between stars, along with the scientific value of the resulting planets. The CTL was constructed to permit a quantitative relative ranking of the best stars to select for the 2-minute cadence slots, not to identify all stars with detectable planets. While in this work we have adopted the set of several million stars in the CTL as the primary sample to investigate, stars not in the CTL might also yield some planet detections in the FFI data. The reason we adopted this approach is the same reason for the construction of the CTL in the first place—our analysis of planet yield among a population of several million stars is much more tractable than conducting the analysis for all 470 million stars in TIC-6.

Explicitly removed from the CTL are stars with an RPM that flags them as giants, stars with parallax or other information that flags them as giants or subgiants, dwarf stars that are somewhat hot and relatively faint but not as faint as some dwarf stars that are included, and faint dwarf stars. The magnitude cut used in the CTL is *TESS* magnitude of 12 for stars hotter than 5500 K and *TESS* magnitude of 13 for cooler stars, although faint cool dwarfs are explicitly included via a specially curated target list (Muirhead et al. 2018). The CTL therefore generally excludes hot stars, faint stars, and evolved stars, in favor of bright, cool dwarfs.

Only a handful of transiting planets have been detected around red giants (e.g., Burrows et al. 2000; Huber et al. 2013; Barclay et al. 2015; Grunblatt et al. 2016; Van Eylen et al. 2016; Grunblatt et al. 2017) because finding these planets is extremely challenging. Transit depth scales with the square of the stellar radius, so planets orbiting large stars are hard to find. Therefore, the frequency of planets orbiting giant stars is relatively poorly constrained. However, *TESS* will observe hundreds of thousands of red giants brighter than 11th mag in the *TESS* bandpass (Huber 2017) and will certainly detect planets orbiting these stars. However, *Kepler* observed roughly 16,000 red giants (Yu et al. 2018) and found only a handful of planets. With a factor 20 or so increase in the number of red giants from *TESS*, we might expect of order 100 new planets. This estimate is comparable to that of Campante et al. (2016), who performed a much more careful analysis and predicted that *TESS* will find roughly 50 planets orbiting red giants.

The brightness cuts applied to the TIC in creating the CTL have a larger impact on our yield estimates. At 12th mag the *TESS* 1 hr integrated noise level is 600 ppm. This equates to detecting a Neptune-size planet with three transits around a solar-radius star, while at 13th mag the noise is 1200 ppm, which is equivalent to a 6 $R_\oplus$ planet. So it is certainly the case that many stars not included in the CTL may have planets detectable with *TESS*. To detect a Jupiter with three transits around a Sun-like star would require a maximum 1 hr integrated noise of approximately 4000 ppm, which corresponds to a *TESS* magnitude of 14.7. The TIC lists 16.0 million stars with temperatures above 5500 K, $\log g$ above 3.9, and *TESS* magnitude of 12–14.7 and 4.2 millions stars with temperature between 4000 and 5500 K, $\log g$ above 4.2, and brightness between 13 and 14.7 (where we cut at 4000 K because the cooler stars are included via the cool star curated list). In our fiducial sample, the frequency of detected planets larger than 4 $R_\oplus$ was 0.069%. Assuming an equal detection rate for fainter stars in the 4+ $R_\oplus$ bin as for brighter stars, we would expect to find 14,000 additional giant planets. Even under our conservative model, the rate is 0.050%, or 10,000 additional planets.

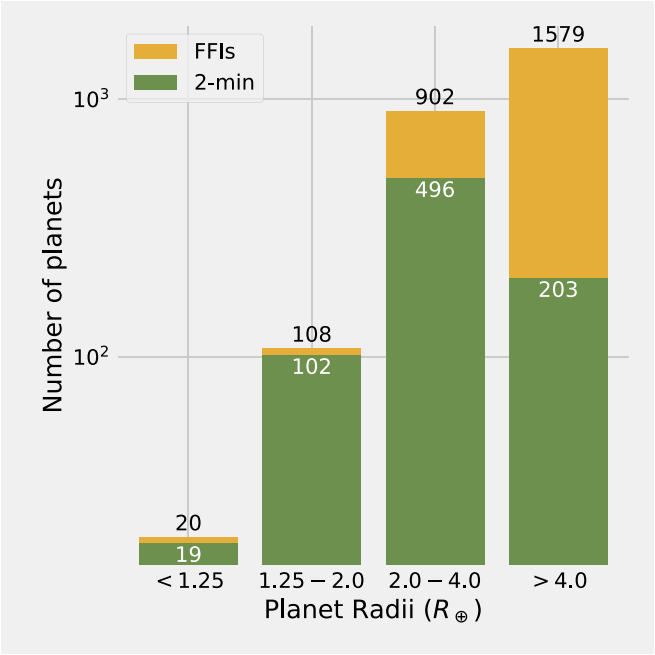

Figure 12. Predicted planet radius distribution using our conservative detection model where we required at least three transits and a combined S/N of 10. This figure is the counterpart of Figure 5, but using our conservative detection model. The total number of planets shown is 2609, which is roughly 60% lower than our standard detection model. This change is most significant for small planets, which saw a factor of two decrease. We have intentionally changed the color scheme from previous figures to differentiate between standard and conservative models.

While these planets will appear in the FFI data, they are not prime targets, hence their exclusion from the CTL, because the planets will be hard to detect and harder to follow up and confirm owing to their faintness and higher crowding. Using the logic described in Section 4.5, the astrophysical false-positive rate in this part of the parameter space is also very high. With a hit rate around 0.05% and a false-positive rate likely to be comparable to that found by Sullivan et al. (2015) of 1 per 180 stars observed, we expect a factor of more than 11-to-1 false-positive to true planets detected. Thus, we caution that searching for planets in this regime is fraught with challenges.

The omission of these potential host stars from our analysis leads to a large underestimate in the overall planet yield of the mission, although that is almost entirely in the giant-planet regime. In Figure 13 we show our final distribution of planet radii and include the sample of giant planets orbiting faint stars, using the conservative yield estimate. This results in a total planet yield of 14,000 transiting planets. However, as discussed, these planets will be resource intensive both to confirm and to meaningfully analyze.

One further source of additional planets is from M dwarfs in the southern hemisphere. As mentioned in Section 2.1, there is

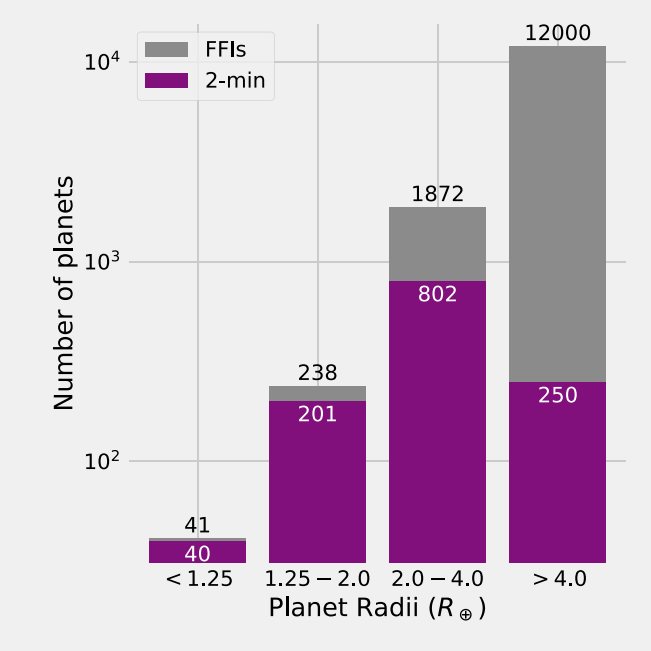

Figure 13. Predicted planet radius distribution including large planets orbiting faint stars outside of the CTL. The total number of planets that we predict *TESS* could find is up to 14,000. This figure is the same as Figure 5 but includes the additional large planets orbiting faint stars. We have intentionally changed the color scheme from previous figures to differentiate from our simulated yield.

a deficit of cool stars below $-30°$ declination, caused primarily by the lower completion of proper-motion catalogs where Northern Hemisphere telescopes are unable to observe. This manifests in fewer planets detected around cool stars in the south. In the 2-minute cadence data, there are 2.6× as many planets orbiting stars cooler than 3900 K north of declination $30°$ than south of declination $-30°$. Including the FFI planets, this increases to 3× as many northern as southern planets (233 vs. 74 planets). With *GAIA* data release 2 now available, it is probable that new M dwarfs in the south will be identified. This will help to recover additional planets orbiting cool stars not identified as dwarfs in the CTL. Given that this could potentially yield new candidate planets for *JWST*, there is a pressing need for this work.

4.7. Comparisons with Earlier Estimates

Sullivan et al. (2015), Bouma et al. (2017), and Ballard (2018) have previously estimated the planet yield from *TESS*. These previous studies selected stars from a simulated Galactic model rather than real stars, and therefore we expect that there are moderate differences between our predicted yields and previous studies. Additionally, we used different selection strategies for both 2-minute cadence targets and FFI stars. We built a realistic 2-minute cadence star selection model that limits the stars observed at the pole cameras to just 6000 stars per hemisphere, whereas the previous works assumed that *TESS* can observe many more stars in the CVZ than is possible with the flight hardware configuration used. We also use a different prioritization metric than previous work, which is based on the metric used by the *TESS* Target Selection Working Group. For the FFI targets we primarily consider those within the CTL, whereas different cuts on brightness are made in earlier works. Therefore, we expect to see significant differences in the planet yield for giant planets.

Sullivan et al. predicted 1700 planets in 2-minute cadence data, of which 560 are smaller than 2 $R_\oplus$. Bouma et al. used the same methodology and software as Sullivan et al. but fixed a number of software bugs and modified a number of parameters. They also predicted 1700 planets from 2-minute cadence data, of which 430 were smaller than 2 $R_\oplus$. The total 2-minute cadence planet yield in both these studies was about 30% larger than we have predicted, but the number of planets smaller than 2 $R_\oplus$ in our study is lower by a factor of 1.7 and 2.3 than Bouma et al. and Sullivan et al. respectively. However, given the different selection strategies, it may be more reasonable to compare the combined 2-minute cadence and FFI yields. Where Bouma et al. (2017) and Sullivan et al. (2015) differ is in their star selection for FFI targets. Bouma et al. limit their selection to the top ranked 3.8 million stars using a similar priority metric to the one applied in CTL 6.1. This enables easy comparison with our 3.2 million star sample. On the other hand, Sullivan et al. (2015) consider all stars brighter than $K_s = 15$, totaling 150 million stars, which we can compare with our analysis in Section 4.6.

Our total simulated yield is remarkably similar to Bouma et al., with 41 versus 49 Earth-sized planets, 238 versus 390 super-Earths, 1900 versus 2000 mini-Neptunes, and 2200 versus 2500 giant planets, for this work and Bouma et al., respectively. The only area where we see a significant deviation is for super-Earths, which we attribute to differences between the Galactic model and real stars.

Compared to Sullivan et al. (2015, 2017), we predict lower totals in all bins. However, as mentioned by Bouma et al., the number of Earths and super-Earths is overestimated by around 30% owing to a bug in their calculation of the dilution from background stars. Taking this into account, our number of Earths matches both Bouma et al. and Sullivan et al., while the super-Earths are comparable. Our rate of giant planets predicted in Section 4.6 is consistent with Sullivan et al.

Ballard used the framework and detection rates of Sullivan et al. (2015) but focused entirely on M1–M4 dwarfs and made significant changes to the occurrence rates to account for covariances between planets in the same systems. In comparison, our analysis of the M dwarf population is simplistic. Ballard predicted a 50% increase in the rate of planets orbiting these cool stars compared to the occurrence rates used by Sullivan et al. (and this work). They predicted 990 ± 350 planets around M1–M4 stars, while we predicted 410 planets orbiting stars with temperatures of 3100–3800 K. If the Ballard occurrence rate has a similar impact on our yields to what it had on Sullivan et al., and given comparable yields between our studies, we would expect an additional 50% of planets in this parameter space, which is 200 more planets orbiting cool stars. Assuming that the increase is uniform in planet size, we might expect an increased yield that includes 14 additional Earths, 42 additional super-Earths, and 142 additional mini-Neptunes. The yield could be even higher if we are able to identify additional M dwarfs in the southern sky, as discussed in Section 4.6.

5. Conclusions

The *TESS* mission will find a large number of transiting planets. However, up until recently the number and physical

properties of the planets that will be discovered have been estimated using simulations performed before the *TESS* observing strategy, 2-minute target list, and flight hardware had been finalized. Here we simulated *TESS* detections of transiting planets using the CTL for our star selection. We have estimated that *TESS* will find more than 14,000 exoplanets, of which 4400 ± 110 orbit stars in the CTL and 1250 ± 70 will be observed at 2-minute cadence. *TESS* will find over 2100 planets smaller than 4 $R_\oplus$, of which 280 will be smaller than 2 $R_\oplus$.

The key design feature that distinguishes *TESS* from *Kepler* is that it will observe brighter stars, emphasizing finding planets that can be followed up more readily from the ground. *TESS* planets range in *V*-band brightness from 4 to 20, with 80% of predicted planets orbiting stars brighter than $V = 13.0$. Assuming $V = 12$ as the limit for recovery of a mass via precision RV observations, we predict that *TESS* will have a sample of 2500 planets for RV observations, of which 1300 will be smaller than 4 $R_\oplus$ and 150 smaller than 2 $R_\oplus$. This will provide a plethora of planets to characterize; the *TESS* follow-up observers should have little problem meeting mission requirements of measuring the masses of 50 planets smaller than 4 $R_\oplus$. We predict that *TESS* will find seven planets orbiting stars brighter than 55 Cnc, the brightest transiting planet host.

There is significant interest in finding habitable zone planets from *TESS*. We predict that around 70 habitable zone planets will be detected and all will orbit M dwarfs, with nine habitable zone planets in our simulations with radii smaller than twice that of Earth's. Our simulations predict that *TESS* will find 70 planets orbiting bright mid-M dwarfs ($K_s < 10$, M3V or later), 10 of which fall into the optimistic habitable zone, making them prime *JWST* targets.

We have shown that nearly all planets valuable for contributing to mission goals related to RV and *JWST* targets will be found in 2-minute cadence data. This is to the great credit of the teams that worked to create the CTL. The availability of 2-minute cadence data will permit more accurate measurements of the radii and orbital configurations of the detected planets. We explored how target selection choices affect the target yield and find that the distribution of targets between the CVZ and shorter observing baseline is well balanced between collecting 2-minute cadence data for the maximum number of planets and finding long-period planets.

There are a large number of stars that are not in the CTL that might host a detectable planet. These stars were intentionally not included in the CTL, and for good reason. They are unlikely to host detectable small planets, and any planets found will be hard to follow up. While there may be as many as 10,000 additional giant planets around the faint stars in the *TESS* data, we have shown that the astrophysical false-positive rate might be as high as 11 false positives per true planet, and there may be as few as one planet detected per 2000 stars searched. While less severe, we anticipate a high astrophysical false-positive rate for stars on the CTL but not included in the 2-minute cadence sample because the ratio of detected planets to stars observed is five times lower than for stars observed at 2-minute cadence.

The mission's target of finding planets with $S/N \geqslant 7.3$ and only two transits may be overly aggressive, based on experience with *Kepler* and *K2* data. We explored an alternative model that applied more conservative detection thresholds of $S/N \geqslant 10$ and requiring three transits. This results in a decrease in the yield estimate of approximately 50% for planets smaller than 4 $R_\oplus$ and occurs across all parameter spaces considered. However, even if this conservative model is realized, more than enough planets will be found to ensure mission success.

This work builds on studies by Sullivan et al. (2015) and Bouma et al. (2017) and would not be possible without their efforts. We do see a moderate decrease from previous yield estimates, although our numbers are remarkably similar to those Bouma et al. presented, considering the different stellar selection strategies.

It will not be long before *TESS* planets are discovered. The real excitement will come from learning about these new worlds using data from ground- and space-based facilities. The legacy of *TESS* will be a catalog of the planets that will be the touchstone planets for years to come. *TESS* will discover which of our nearest stellar neighbors have transiting planets. The brightest host star in our simulation is 70 Oph A, where we recovered a simulated Earth-sized planet. Were this simulation real, on a clear night from a dark site we could point to this star and tell our friends, "that star there has a planet."

This work has been made possible through the valiant efforts of the *TESS* Target Selection Working Group. Without their dedicated effort to create such a high-quality catalog, this work would not be possible. We thank Luke Bouma, Chelsea Huang, Joshua Schlieder, Daniel Huber, Scott Gaudi, Diana Dragomir, Steven Villanueva, Laura Mayorga, Careloine Morley, Laura Kreidberg, and Dana Louie for insightful discussions that greatly improved the manuscript. We also want to recognize the *TESS* team at MIT for their tireless work in making the mission happen. This research has made use of the NASA Exoplanet Archive, which is operated by the California Institute of Technology, under contract with the National Aeronautics and Space Administration under the Exoplanet Exploration Program. This work has made use of the CTL, through the *TESS* Science Office's target selection working group (architects K. Stassun, J. Pepper, N. De Lee, M. Paegert, R. Oelkers). The Filtergraph data portal system is trademarked by Vanderbilt University.

Software: Matplotlib (Hunter 2007), SciPy (Oliphant 2007), NumPy (van der Walt et al. 2011), IPython (Perez & Granger 2007), Jupyter (Kluyver et al. 2016), Pandas (McKinney 2010), Astropy (Astropy Collaboration et al. 2013), Astroquery (Ginsburg et al. 2016), tvguide (Mukai & Barclay 2017), coco (Barclay 2018).

Appendix
Planet Radius as a Function of Distance

Zach Berta-Thompson created a figure using data from Sullivan et al. (2015) that has been widely shared because it is both informative of *TESS*'s capabilities and aesthetically pleasing. We have reproduced Berta-Thompson's plot in Figure 14, with our revised *TESS* yield estimates.

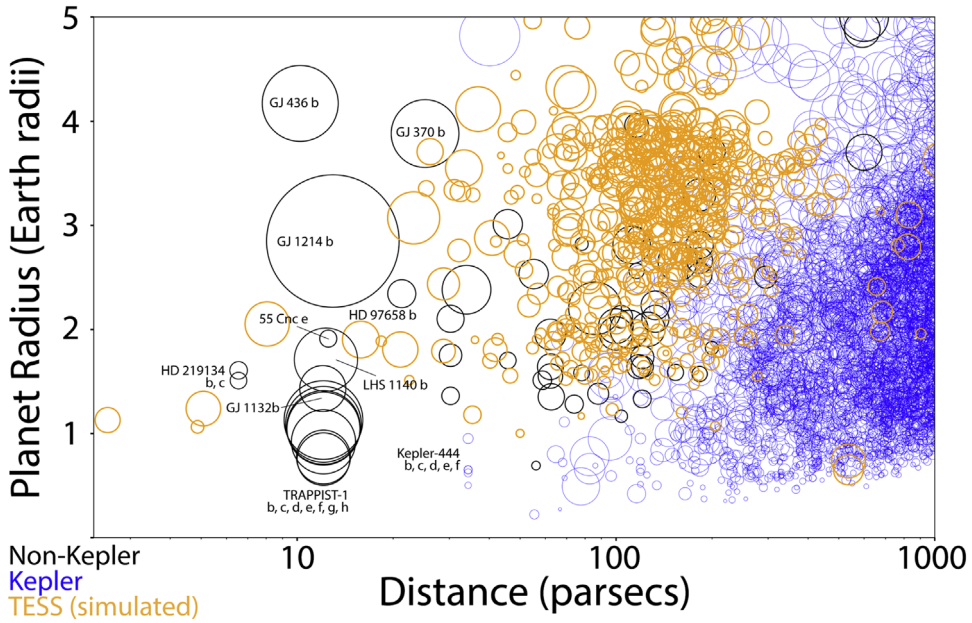

Figure 14. Orbital distance vs. planet radii. This plot updates a widely shared figure created by Z. Berta-Thompson, to now include our new simulation results. *Kepler* planet candidates from Thompson et al. (2018) are shown in blue, our simulated 2-minute cadence detections in orange, and planets detected using other telescopes in black. The size of the circle is proportional to the transit depth. A subset of nearby planets are marked. Data were extracted from the Exoplanet Archive (Akeson et al. 2013). Three planets in our simulation orbit stars closer than the nearest known transiting planet system HD 219134.

ORCID iDs

Thomas Barclay https://orcid.org/0000-0001-7139-2724
Joshua Pepper https://orcid.org/0000-0002-3827-8417
Elisa V. Quintana https://orcid.org/0000-0003-1309-2904

References

Akeson, R. L., Chen, X., Ciardi, D., et al. 2013, PASP, 125, 989
Armstrong, D. J., Pollacco, D., & Santerne, A. 2017, MNRAS, 465, 2634
Astropy Collaboration, Robitaille, T. P., Tollerud, E. J., et al. 2013, A&A, 558, A33
Ballard, S. 2018, arXiv:1801.04949
Barclay, T. 2018, coco: Command line tool to get coordinates for astronomical sources, Zenodo, doi:10.5281/zenodo.1216241
Barclay, T., Endl, M., Huber, D., et al. 2015, ApJ, 800, 46
Batalha, N. E., Mandell, A., Pontoppidan, K., et al. 2017, PASP, 129, 064501
Bonfils, X., Delfosse, X., Udry, S., et al. 2013, A&A, 549, A109
Borucki, W. J., Koch, D., Basri, G., et al. 2010, Sci, 327, 977
Bouma, L. G., Winn, J. N., Kosiarek, J., & McCullough, P. R. 2017, arXiv:1705.08891
Burke, C. J., Christiansen, J. L., Mullally, F., et al. 2015, ApJ, 809, 8
Burrows, A., Guillot, T., Hubbard, W. B., et al. 2000, ApJL, 534, L97
Campante, T. L., Schofield, M., Kuszlewicz, J. S., et al. 2016, ApJ, 830, 138
Campbell, B., Walker, G. A. H., & Yang, S. 1988, ApJ, 331, 902
Catanzarite, J., & Shao, M. 2011, ApJ, 738, 151
Christiansen, J. L., Clarke, B. D., Burke, C. J., et al. 2016, ApJ, 828, 99
Clanton, C., & Gaudi, B. S. 2016, ApJ, 819, 125
Collier Cameron, A., Wilson, D. M., West, R. G., et al. 2007, MNRAS, 380, 1230
Collins, K. A., Collins, K. I., Pepper, J., et al. 2018, arXiv:1803.01869
Crossfield, I. J. M., Ciardi, D. R., Petigura, E. A., et al. 2016, ApJS, 226, 7
Crossfield, I. J. M., Petigura, E., Schlieder, J. E., et al. 2015, ApJ, 804, 10
Crouzet, N., Bonfils, X., Delfosse, X., et al. 2017, arXiv:1701.03539
Davenport, J. R. A. 2017, ApJ, 835, 16
Dressing, C. D., & Charbonneau, D. 2013, ApJ, 767, 95
Dressing, C. D., & Charbonneau, D. 2015, ApJ, 807, 45
Foreman-Mackey, D., Hogg, D. W., & Morton, T. D. 2014, ApJ, 795, 64
Fressin, F., Torres, G., Charbonneau, D., et al. 2013, ApJ, 766, 81
Gillon, M., Triaud, A. H. M. J., Demory, B.-O., et al. 2017, Natur, 542, 456
Ginsburg, A., Parikh, M., Woillez, J., et al. 2016, Astroquery, v0.3.1, Zenodo, doi:10.5281/zenodo.44961
Gould, A., Dong, S., Gaudi, B. S., et al. 2010, ApJ, 720, 1073
Greene, T. P., Line, M. R., Montero, C., et al. 2016, ApJ, 817, 17
Grunblatt, S. K., Huber, D., Gaidos, E., et al. 2017, AJ, 154, 254
Grunblatt, S. K., Huber, D., Gaidos, E. J., et al. 2016, AJ, 152, 185
Howard, A. W., Marcy, G. W., Bryson, S. T., et al. 2012, ApJS, 201, 15
Howard, A. W., Marcy, G. W., Johnson, J. A., et al. 2010, Sci, 330, 653
Howell, S. B., Sobeck, C., Haas, M., et al. 2014, PASP, 126, 398
Hsu, D. C., Ford, E. B., Ragozzine, D., & Morehead, R. C. 2018, AJ, 155, 205
Huber, D. 2017, Asteroseismic Red Giant Yield for TESS, figshare, doi:10.6084/m9.figshare.4883804.v1
Huber, D., Carter, J. A., Barbieri, M., et al. 2013, Sci, 342, 331
Huber, D., Silva Aguirre, V., Matthews, J. M., et al. 2014, ApJS, 211, 2
Huber, D., Zinn, J., Bojsen-Hansen, M., et al. 2017, ApJ, 844, 102
Hunter, J. D. 2007, CSE, 9, 90
Jenkins, J. M., Caldwell, D. A., Chandrasekaran, H., et al. 2010, ApJL, 713, L87
Kane, S. R., Kopparapu, R. K., & Domagal-Goldman, S. D. 2014, ApJL, 794, L5
Kempton, E. M.-R., Bean, J. L., Louie, D. R., et al. 2018, PASP, 130, 114401
Kipping, D. M. 2014, MNRAS, 444, 2263
Kipping, D. M., & Lam, C. 2017, MNRAS, 465, 3495
Kluyver, T., Ragan-Kelley, B., Pérez, F., et al. 2016, in Positioning and Power in Academic Publishing: Players, Agents and Agendas, ed. F. Loizides & B. Scmidt (Amsterdam: IOS Press), 87
Koch, D. G., Borucki, W. J., Basri, G., et al. 2010, ApJL, 713, L79
Kopparapu, R. K., Ramirez, R., Kasting, J. F., et al. 2013, ApJ, 765, 131
Koppenhoefer, J., Saglia, R. P., Fossati, L., et al. 2013, MNRAS, 435, 3133
Kreidberg, L., & Loeb, A. 2016, ApJL, 832, L12
Latham, D. W., Stefanik, R. P., Mazeh, T., Mayor, M., & Burki, G. 1989, Natur, 339, 38
Lissauer, J. J., Marcy, G. W., Rowe, J. F., et al. 2012, ApJ, 750, 112
Lopez, E. D., & Fortney, J. J. 2014, ApJ, 792, 1
Louie, D. R., Deming, D., Albert, L., et al. 2018, PASP, 130, 044401
Lund, M. N., Handberg, R., Kjeldsen, H., Chaplin, W. J., & Christensen-Dalsgaard, J. 2017, EPJWC, 160, 01005
Mathur, S., Huber, D., Batalha, N. M., et al. 2017, ApJS, 229, 30
Mayor, M., & Queloz, D. 1995, Natur, 378, 355
Mayorga, L. C., & Thorngren, D. P. 2018, RNAAS, 2b, 40
McKinney, W. 2010, in Proc. 9th Python in Science Conf., ed. S. van der Walt & J. Millman, 51
Montet, B. T., Crepp, J. R., Johnson, J. A., Howard, A. W., & Marcy, G. W. 2014, ApJ, 781, 28
Morley, C. V., Kreidberg, L., Rustamkulov, Z., Robinson, T., & Fortney, J. J. 2017, ApJ, 850, 121
Morton, T. D., & Swift, J. 2014, ApJ, 791, 10
Muirhead, P. S., Dressing, C. D., Mann, A. W., et al. 2018, AJ, 155, 180

Mukai, K., & Barclay, T. 2017, Tvguide: A tool for determining whether stars and galaxies are observable by TESS, Zenodo, doi:10.5281/zenodo.823357
Mulders, G. D., Pascucci, I., & Apai, D. 2015, ApJ, 814, 130
Mullally, F., Thompson, S. E., Coughlin, J. L., Burke, C. J., & Rowe, J. F. 2018, AJ, 155, 210
Oelkers, R. J., & Stassun, K. G. 2018, AJ, 156, 132
Oliphant, T. E. 2007, CSE, 9, 10
Pecaut, M. J., & Mamajek, E. E. 2013, ApJS, 208, 9
Perez, F., & Granger, B. E. 2007, CSE, 9, 21
Petigura, E. A., Howard, A. W., & Marcy, G. W. 2013a, PNAS, 110, 19273
Petigura, E. A., Marcy, G. W., & Howard, A. W. 2013b, ApJ, 770, 69
Ricker, G. R., Vanderspek, R., Winn, J., et al. 2016, Proc. SPIE, 9904, 99042B
Ricker, G. R., Winn, J. N., Vanderspek, R., et al. 2015, JATIS, 1, 014003
Sanchis-Ojeda, R., Rappaport, S., Winn, J. N., et al. 2013, ApJ, 774, 54
Shapley, H. 1953, The Climatic Change: Evidence Causes, and Effects (Cambridge, MA: Harvard Univ. Press)
Stassun, K. G., Corsaro, E., Pepper, J. A., & Gaudi, B. S. 2018, AJ, 155, 22
Stassun, K. G., Oelkers, R. J., Pepper, J., et al. 2017, arXiv:1706.00495
Strughold, H. 1953, The Green and Red Planet; a Physiological Study of the Possibility of Life on Mars (Albuquerque, NM: Univ. New Mexico Press)
Sullivan, P. W., Winn, J. N., Berta-Thompson, Z. K., et al. 2015, ApJ, 809, 77
Sullivan, P. W., Winn, J. N., Berta-Thompson, Z. K., et al. 2017, ApJ, 837, 99
Swift, J. J., Johnson, J. A., Morton, T. D., et al. 2013, ApJ, 764, 105
Thompson, S. E., Coughlin, J. L., Hoffman, K., et al. 2018, ApJS, 235, 38
Thorngren, D. P., & Fortney, J. J. 2018, AJ, 155, 214
Traub, W. A. 2012, ApJ, 745, 20
van der Walt, S., Colbert, S. C., & Varoquaux, G. 2011, CSE, 13, 22
Van Eylen, V., & Albrecht, S. 2015, ApJ, 808, 126
Van Eylen, V., Albrecht, S., Gandolfi, D., et al. 2016, AJ, 152, 143
Vanderburg, A., Montet, B. T., Johnson, J. A., et al. 2015, ApJ, 800, 59
Villanueva, S., Jr., Dragomir, D., & Gaudi, B. S. 2018, arXiv:1805.00956
Vinícius, Z., Barentsen, G., Gully-Santiago, M., et al. 2017, KeplerGO/PyKE, Zenodo, doi:10.5281/zenodo.835583
Winn, J. N. 2010, in Exoplanet Transits and Occultations, ed. S. Seager (Tucson, AZ: Univ. Arizona Press), 55
Winn, J. N., Matthews, J. M., Dawson, R. I., et al. 2011, ApJL, 737, L18
Winn, J. N., Sanchis-Ojeda, R., & Rappaport, S. 2018, arXiv:1803.03303
Wolszczan, A., & Frail, D. A. 1992, Natur, 355, 145
Xie, J.-W., Dong, S., Zhu, Z., et al. 2016, PNAS, 113, 11431
Youdin, A. N. 2011, ApJ, 742, 38
Yu, J., Huber, D., Bedding, T. R., et al. 2018, ApJS, 236, 42